Simultaneous enhancement of strength and ductility in an AlCoCrFeNi$_{2.1}$ eutectic high-entropy alloy via friction stir processing

Tianhao Wang, Mageshwari Komarasamy, Shivakant Shukla, Rajiv S. Mishra[*]
Center for Friction Stir Processing and Advanced Materials Manufacturing Processing Institute,
Department of Materials Science and Engineering,
University of North Texas, Denton, TX 76203, USA
*Corresponding author: email ID — Rajiv.Mishra@unt.edu

Abstract

Lamellar eutectic structure of as-cast AlCoCrFeNi$_{2.1}$ was tailored by friction stir processing (FSP). During FSP, lamellar B2 phase was broken into ultrafine-grained particles, with dissolution of Cr-rich precipitates in B2 and formation of Al-rich precipitates in FCC (L1$_2$). Dynamic recrystallization of FCC/L1$_2$ and B2 reduced grain size to less than ~0.5 μm. The combined effect of microstructural evolution in the processed region improved the ultimate tensile strength from ~1000 MPa to 1360 MPa, the ductility from ~6.5% to 10%, and the microhardness from ~300 HV0.2 to 450 HV0.2.

Key words: eutectic high-entropy alloy; friction stir processing; strength; ductility; precipitate; hardness

1. Introduction

Multicomponent high-entropy alloys (HEAs) as first conceptualized and synthesized in 2004 consisted of five or more principal elements in equiatomic or non-equiatomic composition to maximize the configurational entropy of mixing [1,2]. In addition to single-phase alloys, compositions forming second phases and intermetallic compounds are now included and are designated as complex concentrated alloys (CCAs) [3]. Single phases alloys including face-centered cubic (FCC) or body-centered cubic (BCC) or hexagonal close packed (HCP), and multi-phase systems including FCC+BCC have been developed since 2004 [3]. In AlCoCrFeNi$_{2.1}$ HEA composition, a lamellar eutectic structure composed of B2 (BCC, NiAl rich precipitates) and FCC (L1$_2$) phases with semi-coherent interface was produced, and is known as eutectic high-entropy alloy (EHEA) [4]. EHEA combines high strength of BCC phase and high ductility of FCC phase, hence becoming one of the most promising alloys in terms of attaining optimum strength-ductility combination. Furthermore, Cr-rich coherent precipitates are present in B2 lamellae. The remarkable combination of ultimate tensile strength (1351 MPa) and tensile ductility (15.4%) was achieved in cast EHEAs [5]. During tensile testing on EHEAs, the FCC phase deformed via planar dislocation slip (slip system is {111} <110>) and stacking faults due to low stacking fault energy (SFE) that leads to high ductility in EHEAs. Strengthening of the B2 phase originated from high-density dislocations pinned by the Cr-rich nano-precipitates on two of {110} slip bands [5]. However, in coarse lamellar eutectic structure with strength mismatch, dislocation accumulation and subsequent crack nucleation along FCC/B2 phase boundaries propagated into the B2 phase and led to B2 fracture. The FCC (L1$_2$) phase finally fractured on further increase in load during tensile testing [5]. Wani et al. [6,7] modified the lamellar eutectic structure by applying cold rolling and annealing treatment. The modified microstructure was

comprised of profuse shear banding, disordering of FCC ($L1_2$) and broken B2 phase [6]. After annealing at 800 to 1200°C, appreciable ductility over 10% as well as high tensile strength greater than 1000 MPa were obtained [7].

Friction sir processing (FSP) as a microstructural modification method has been applied for low melting point materials such as cast aluminum [8] and magnesium [9] alloys with eutectic structures. During FSP, a coarse eutectic β-$Mg_{17}Al_{12}$ phase in matrix was deformed, fractured and dissolved along with matrix grain refinement. In addition, FSP can also break coarse, un-dissolvable Si particles into small ones in Al-Mg-Si alloys. Therefore, the mechanical properties of as-cast material were generally improved due to microstructural modification by FSP. With the advent of W-based [10] or PcBN [11] tools, high melting point materials can also be processed and modified by FSP. In this study, FSP was applied to tailor the as-cast EHEA $AlCoCrFeNi_{2.1}$. Microstructural and phase evolution was investigated using various microscopy techniques. Both strength and ductility were enhanced significantly compared with as-cast material. The effect of aging heat treatment on processed EHEAs was also studied.

2. Experimental procedures

As-cast $AlCoCrFeNi_{2.1}$ plates (~6.0 mm thick) were friction stir processed (FSPed) with PcBN tool. The tool dimensions are: shoulder diameter of 23.8 mm, pin height of 5 mm and pin diameter of 7.6 mm. Tool rotation rate was ranged from 250 to 500 rotation per min (rpm) and traverse speed ranged from 2 to 4 inches per min (ipm). The material processed at 500 rpm and 3 ipm was selected for further characterization. The FSPed sample was subjected to aging heat treatment of 620°C for 8 h to form strengthening precipitates. Transverse cross sections of FSPed and FSPed+aged samples were cut by electrical discharge machining and final polished to 0.02 μm surface finish with colloidal silica suspension. Scanning electron microscopy (SEM) in back-

3

scattered electron mode (BSE) and energy-dispersive X-ray spectroscopy (EDS) analyses of FSPed and FSPed+aged samples were carried out using FEI Nova NanoSEM 230 with EDAX Octane Elite EDS, including EDS elemental mapping. X-ray diffraction (XRD) was used to evaluate FCC and BCC phases in as-cast and FSPed EHEA using Rigaku Ultima III high-resolution XRD with Cu K_{α} radiation. Electron backscatter diffraction (EBSD) analysis of the evolution of FCC (L1$_2$) and B2 (BCC) phases, grain size and grain orientation after FSP was done using Hikari Super EBSD system and TSL OIM^{TM} software. Mini-tensile testing on the as-cast material and FSPed region was conducted at initial strain rate of 0.001 s^{-1}. The width, thickness and gage length of the samples were 1.0, 0.6, and 2.0 mm, respectively. The mini-tensile samples were taken from the middle region of the nugget. Microhardness characterization of FSPed and FSPed+aged samples was conducted on the transverse cross section using Vickers microhardness tester at load of 200 g and dwell time of 10 s.

3. Results and discussion

Lamellar eutectic structure of as-cast EHEA is composed of FCC/L1$_2$ phase (lighter region) and (NiAl) rich B2 phase (darker region (Figure 1 (a)). Grain size of the FCC matrix in as-cast condition exceeded ~300 μm. Furthermore, nano-sized particles (white spots) in the B2 phase are shown in the high magnification image (inset in Figure 1 (a)). Based on literature observations of as-cast EHEAs, these nano particles are Cr-rich precipitates [5,7]. Due to intense high-temperature severe plastic deformation introduced during FSP, B2 lamellae were deformed and broken into small particles (top inset of Figure 1 (b), also denoted by green arrows). The change from continuous lamellar structure to dispersed phase creates an interesting ultrafine-grained (UFG) multiphase microstructure. Furthermore, Cr-rich precipitates that were observed in the as-cast condition were dissolved in the FSPed region due to both severe plastic deformation and

high temperature (Figure 1 (b), marked by green circles). Interestingly, in addition to broken B2, fine, black precipitates also formed in the processed region (top inset of Figure 1 (b), marked by red circles). EDS mapping of the same region presented as another inset (bottom) confirmed that these black precipitates are Al-rich; the same particles are also marked by a red circle in both top and bottom insets. The following explains this observation. In addition to breaking of B2 lamellae into fine particles, intense high temperature severe plastic deformation might have also dissolved some of the (AlNi)-rich B2 phase. FSP has also been used to force mix immiscible elements such as Nb and Ag into the Cu matrix due to intense severe plastic deformation [12]. Therefore, during processing, a certain fraction of the B2 phase being dissolved into the FCC matrix is highly possible. However, thermodynamic factors limiting Al solid solubility in the EHEA matrix might have led to re-precipitation of the Al-rich phase. Furthermore, in the processed region, a broken B2 phase in the retreating side (RS) (Figure 1 (c)) was more clustered and coarser than microstructure in the advancing side (AS) (Figure 1 (b)). This is because the processed volume along AS experienced higher plastic strain than material in RS, which led to a finer B2 phase [13]. The boundary region between the nugget/thermomechanically affected zone (TMAZ) can be regarded as the transition zone that reveals the sequence of B2 lamellae elongation, deformation and then the breaking process (Figure 1 (d)). The same sequence is expected to be present in the material volume that was in contact with the FSP tool and was becoming severely deformed by the tool. Since these processes were happening inside the material volume, the TMAZ region provided an insight into the possible deformation sequence of the lamellar eutectic structure. Both FCC and B2 phases underwent severe straining and upon reaching fracture strain, B2 lamellae broke into fine particles. Furthermore, due to large strain

5

and high temperature, recrystallization of both B2 and FCC phases occurred, as expected, and is presented in the next subsection.
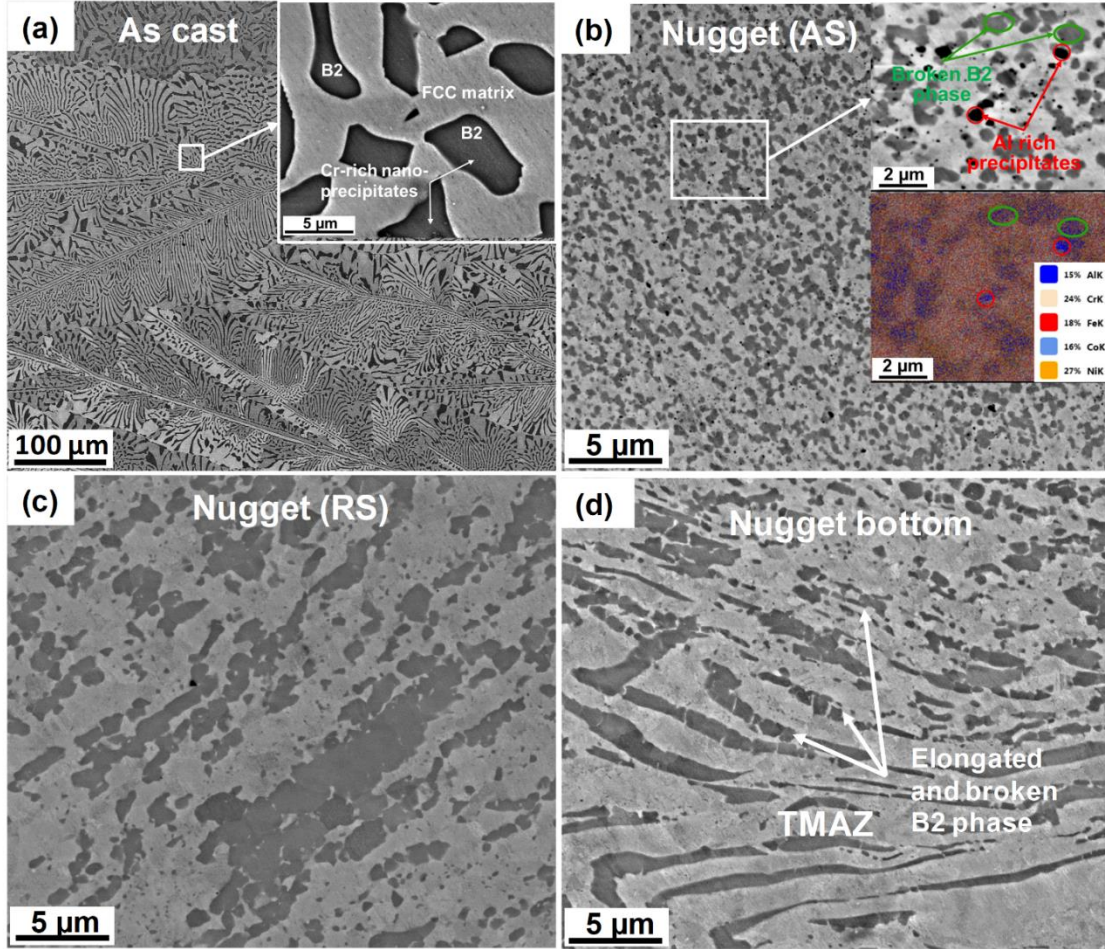

Figure 1. SEM of (a) as-cast EHEA with FCC (L1$_2$) matrix and B2 (BCC) phase with Cr-rich precipitates, (b) FSPed nugget at AS with broken B2 phase (marked by green circles) and Al rich precipitates (marked by red circles), (c) FSPed nugget at RS with clustered and coarse broken B2 phase, and (d) boundary region between nugget bottom/TMAZ with elongated and broken B2 phase. Note the presence and absence of Cr-rich precipitates in as-cast and processed conditions, respectively.

In the as-cast condition, no significant changes in crystal orientation among various B2 lamellae across multiple grains were noted, as can be observed in similar color in the inverse pole figure (IPF) grain orientation map (Figure 2 (a)). Phase map obtained from EBSD characterization is presented in Figure 2 (b) showing the FCC and B2 phase distribution in the as-cast material.

After FSP, the center of the processed volume was selected for EBSD analysis and is shown in Figures 2 (c,d). Due to dynamic recrystallization during FSP, the coarse, lamellar structure was replaced by fine B2 particles exhibiting various grain orientations (Figure 2 (c_2) and (d)). FCC/L1$_2$ (Figure 2(c_1)) and B2 (Figure 2(c_2)) grains were refined to ~0.50 and ~0.46 µm, respectively, by high-temperature severe plastic deformation and dynamic recrystallization. Phase map of the severe plastically deformed volume is given in Figure 2(d). The slight increase in FCC and B2 (BCC) phase fraction in the processed region might be due to location dependency of fractions in the as-cast condition. Some twins were also present within the recrystallized FCC/L1$_2$ grains (white lines in FCC grains in Figure 2 (d)) signifying the low SFE of the FCC matrix). In the case of as-cast microstructure, Kurdjumov-Sachs (K-S) orientation relationship (OR) ($\{111\}_{FCC} // \{110\}_{B2}$, $<1\overline{1}0>_{FCC} // <1\overline{1}1>_{B2}$) between the FCC and B2 phases was observed along all the phase boundaries (blue lines along FCC/B2 interfaces in Figure 2 (b)). On the other hand, due to high temperature intense severe plastic deformation and subsequent dynamic recrystallization during FSP, large fraction of the phase boundaries exhibited a random orientation between the FCC and B2 phases while low fraction of K-S OR (blue lines) and Nishiyama-Wassermann (N-W) OR ($\{111\}_{FCC} // \{110\}_{B2}$, $<0\overline{1}1>_{FCC} // <001>_{B2}$) were also observed denoted by yellow lines in Figure 2 (d)).
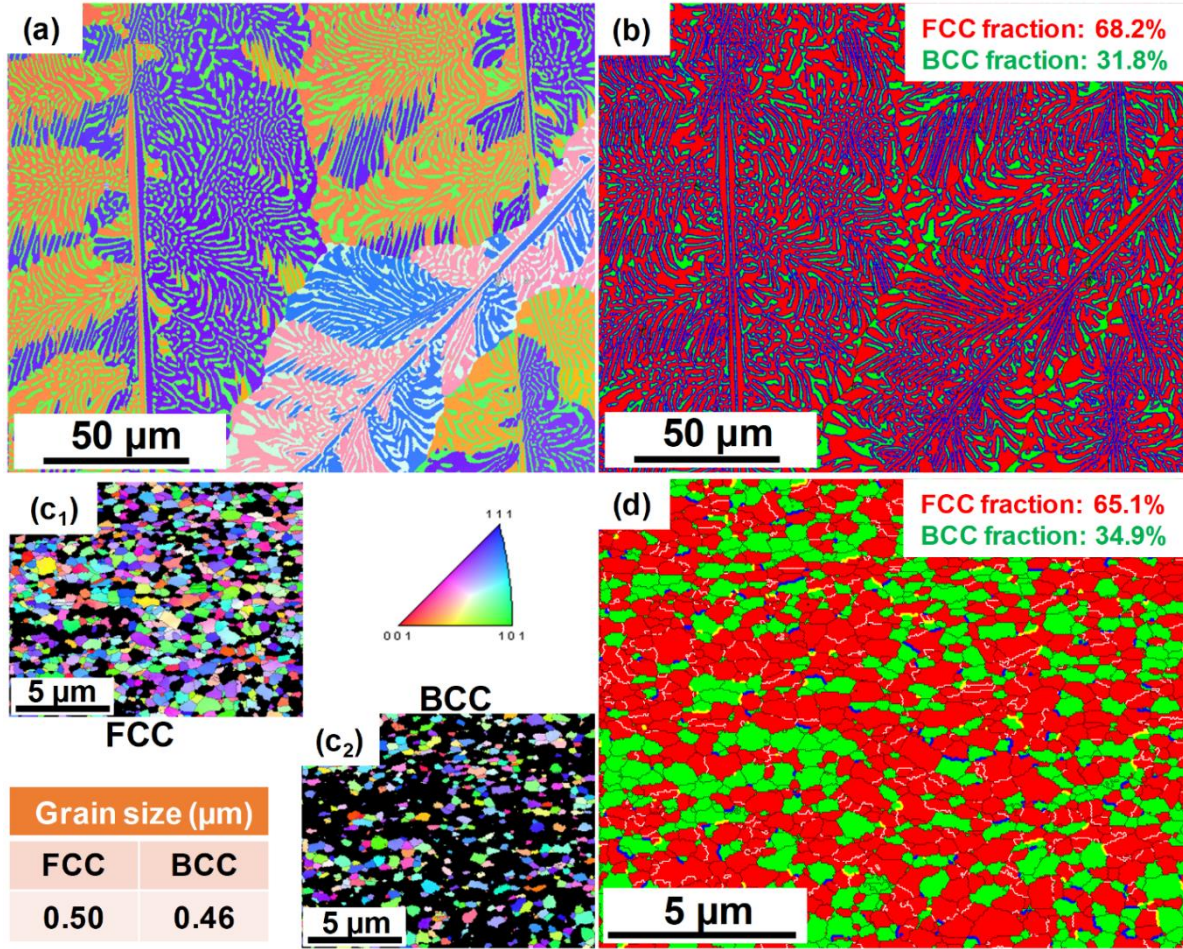
Figure 2. (a) IPF and (b) phase map of as-cast EHEA and IPF of (c₁) FCC/L1₂, (c₂) BCC/B2, and (d) phase map of FSPed EHEA. Note that as-cast microstructure was textured with (111) planes which was replaced by random grain orientation in the processed material. The K-S OR (blue lines in Figure 2 (b)) in as-cast condition was reduced to a very low fraction and some new N-W OR (yellow lines in Figure 2 (d)) appeared. Twins were present within the recrystallized FCC/L1₂ grains (white lines in Figure 2 (d)).

As shown in Figure 3 (a), XRD analysis confirmed that dominant crystal planes for FCC/L1₂ and B2 phases in as-cast EHEA were (111) and (110), respectively, which agreed with IPF results (Figure 2(a)). After dynamic recrystallization following FSP, crystal orientations were random for both FCC/L1₂ and B2 phases (Figure 3 (b)). In addition, a peak of Al_3Ni phase appeared in FSPed condition. There is a possibility that Al-rich precipitates presented in the SEM and EDS map in Figure 2(b) were Al_3Ni.
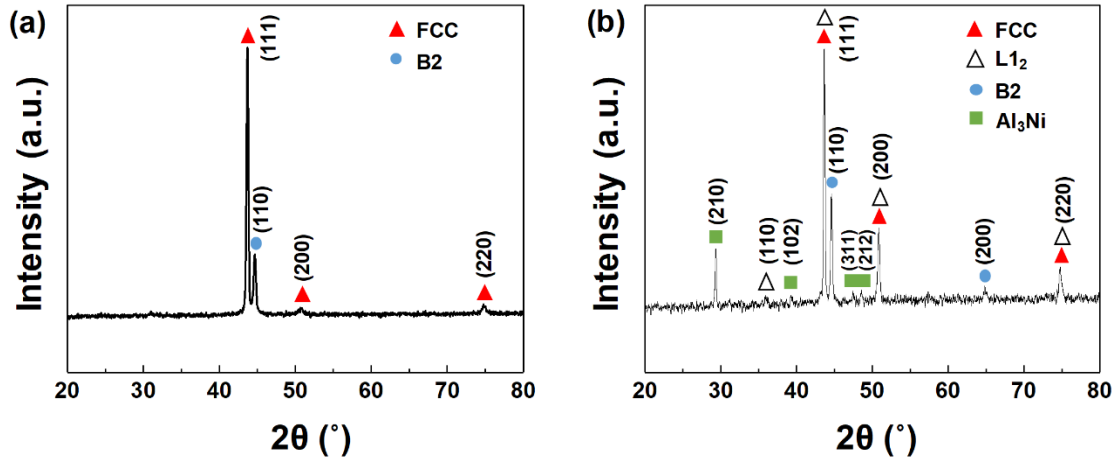
Figure 3. XRD analyses of (a) as-cast EHEA and (b) FSPed EHEA. Note the dominance of (111) and (110) texture in FCC/L12 and B2 phases, respectively, in as-cast condition. Also note the increase in intensity of other peaks in the processed condition.

To study element redistribution after FSP, EDS elemental mapping on as-cast and FSPed samples are displayed in Figure 4. Three regions including B2, FCC1, and FCC2 existed in the as-cast condition (Figure 4 (a)). After FSP, FCC1 and FCC2 merged into a single FCC phase (Figure 4 (b)). Element compositions in FCC (FSPed condition) were between those in FCC1) and FCC2. In addition, the sum of all elements kept constant, the contents of Al and Ni decreased in B2; while Cr, Co, and Fe contents increased compared with as-cast condition.

Element	Sum (at.%)	B2 (at.%)	FCC1 (at.%)	FCC2 (at.%)
Al	15.37	22.56	10.74	15.86
Cr	17.65	12.38	21.46	16.85
Fe	17.67	14.07	19.85	17.58
Co	16.67	14.31	17.97	16.71
Ni	32.64	36.67	29.98	32.99

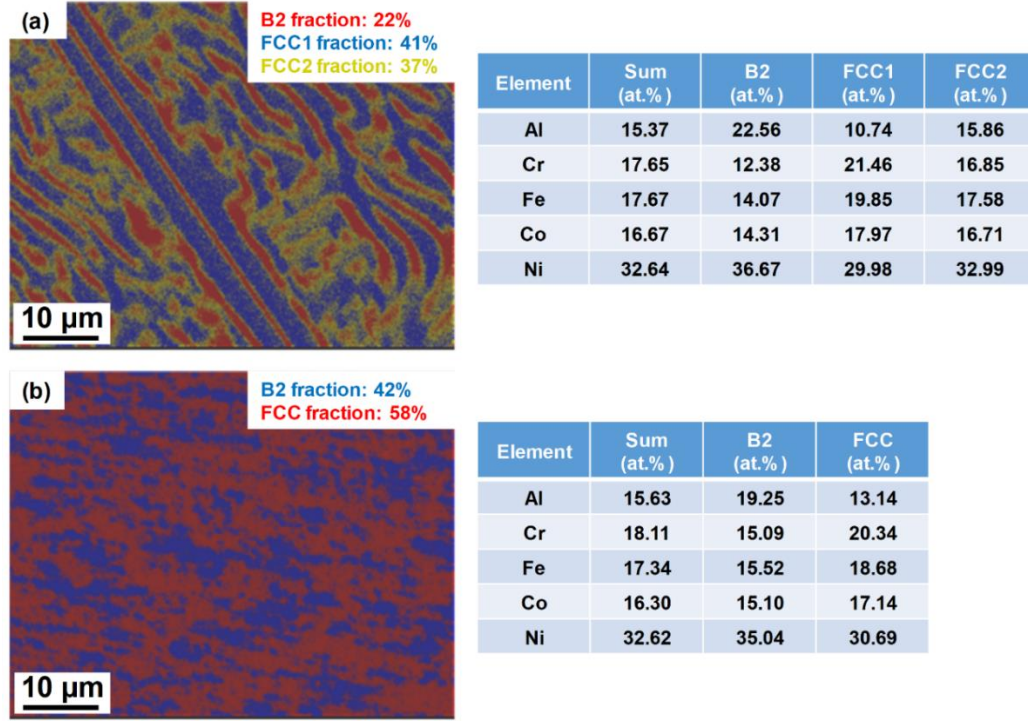| Element	Sum (at.%)	B2 (at.%)	FCC (at.%)
Al	15.63	19.25	13.14
Cr	18.11	15.09	20.34
Fe	17.34	15.52	18.68
Co	16.30	15.10	17.14
Ni	32.62	35.04	30.69

Figure 4. EDS mapping analysis on (a) as-cast and (b) as FSPed EHEA.

The effect of aging heat treatment on precipitation behavior in EHEA was investigated. In the heat affected zone (HAZ) of the FSPed sample, microstructural evolution arises only from the thermal effect. As shown in Figure 5 (a), the eutectic lamellar structure was not coarsened since the peak temperature in HAZ was expected to be (~1000°C [11]) lower than the eutectic temperature of AlCoCrFeNi$_{2.1}$ (1350°C). Furthermore, Cr-rich precipitates that were present in the B2 phase in as-cast condition were dissolved due to the thermal cycle (Figure 5 (a)). Interestingly, after aging at 620°C for 8 h, Cr-rich precipitates formed again in the B2 phase in the HAZ (Figure 5 (c)). In addition to Cr-rich precipitates, dark contrast precipitates also formed inside the B2 phase which could be rich in Al (black particles in Figure 5 (c)). The same observations, i.e., precipitation of both Cr-rich and Al-rich precipitates, were present in the

10

processed region after heat treatment (Figure 5 (d)). Note the absence of secondary precipitates in the broken B2 phase in the FSP region (Figure 5 (b)).
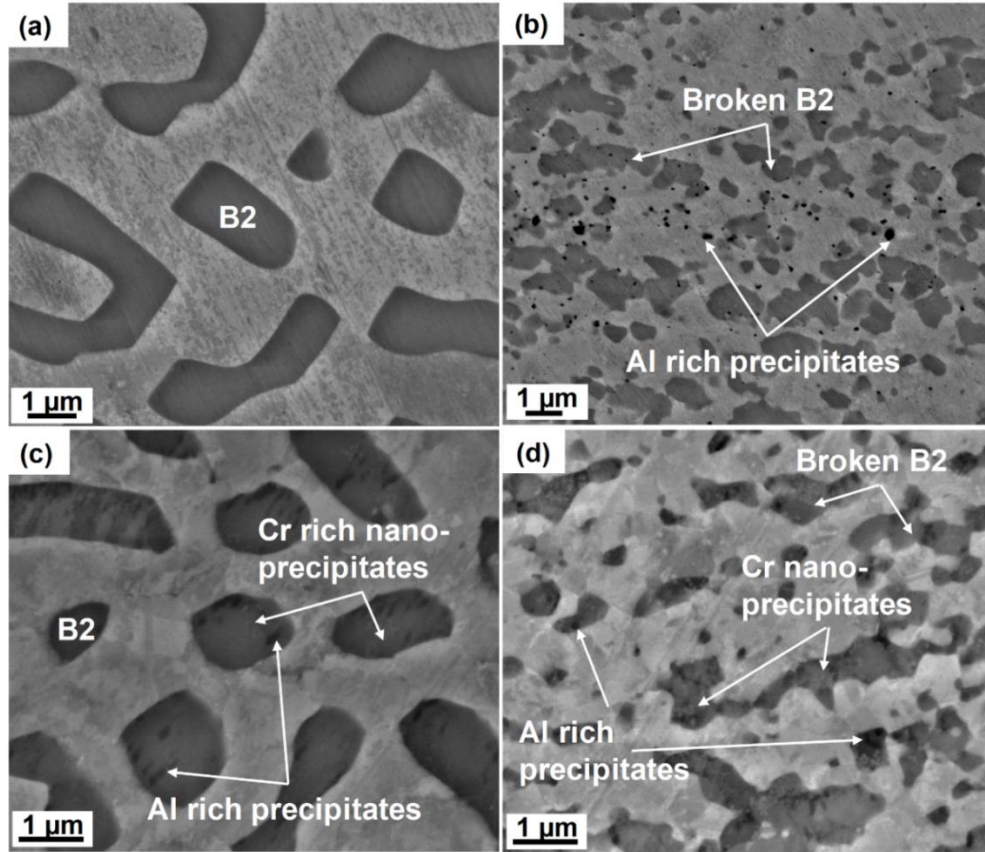

Figure 5. SEM of (a) HAZ and (b) nugget of FSPed sample with precipitates absent in B2 phase, and (c) HAZ and (d) nugget of FSPed+aged condition showing the Cr-rich precipitates and Al-rich precipitates.

Tensile stress-strain curves of the as-cast and FSPed material shows that yield strength and ultimate tensile strength were enhanced from ~800 MPa to 920 MPa and from ~1000 MPa to 1360 MPa, respectively, and the ductility increased from 6.5% to 10% after FSP (Figure 6 (a)). The strength increase originated from UFG structure of FCC/L1$_2$ and B2/BCC phases. Due to the lamellar structure, tensile elongation in the as-cast condition was relatively small. The breakage of the lamellar structure into fine particles reduced the tendency of easy crack propagation along the FCC/B2 phase boundaries in FSPed material. Furthermore, strain hardening mechanism of

11

both as-cast and FSPed HEA is presented in Figure 6 (b). For both conditions, the decrease of work-hardening rate in stage A implies a dynamic recovery controlled regime and stage B is dominated by twinning related deformation mechanisms [13,14]. No further microstructural investigation on the work hardening mechanisms was performed and the analysis made in the current investigation was entirely based on the literature observations. Deformational twinning is expected in both the microstructural conditions due to the low SFE of the FCC matrix. In FSPed HEA, both stages A and B were slightly extended as compared to as-cast material. Overall, the breakage of lamellar structure along with extended deformation regimes led to the observed tensile ductility of 10%.
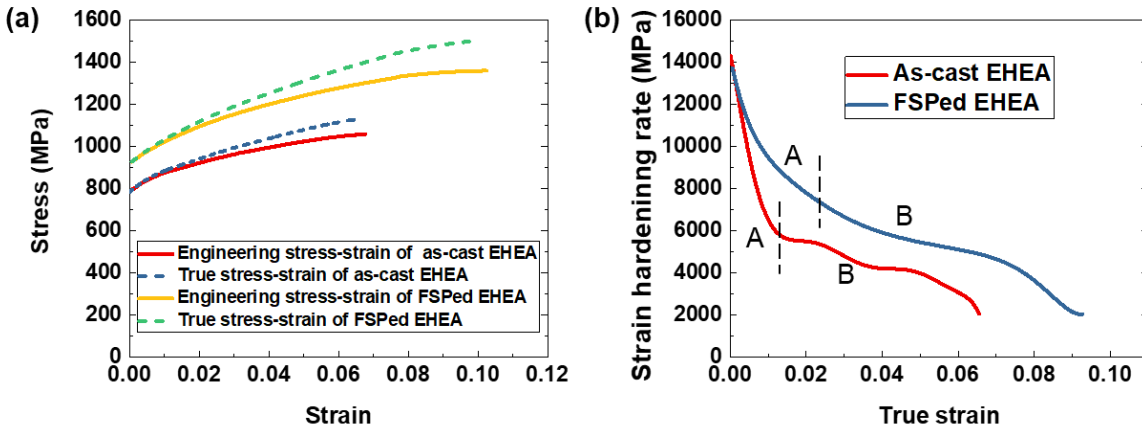

Figure 6. (a) Stress and strain curves and (b) strain hardening rate of as cast and FSPed EHEA.

Microhardness characterization on FSPed and FSPed + aged samples (Figure 7) shows that microhardness increased from ~300 in as-cast condition to ~450 HV0.2 in FSPed nugget. This is because in the FSPed nugget, refinement of FCC/L1$_2$ and B2 into ultrafine-grained regime, and the formation of fine Al-rich precipitates in the FCC matrix increased hardness significantly as compared to the as-cast base material. Furthermore, the hardness in HAZ decreased from ~300 HV0.2 in the as-cast condition to ~250 HV0.2 due to the dissolution of Cr-rich precipitates in the

B2 phase. Hardness difference between AS and RS of the nugget resulted from size variation of B2 particles. In the HAZ of FSPed sample, microhardness decreased from ~300 in as-cast condition to ~255 HV0.2 without noticeable coarsening of B2 lamellae. Hardness value reduction in HAZ of FSPed sample can only be attributed to the dissolution of Cr-rich precipitates in the B2 phase. After aging of the FSPed sample, microhardness in the nugget improved from ~450 in FSPed condition to ~480 HV0.2 in FSPed+aged condition. Hardness increase by aging originated from the re-precipitation of Cr-rich precipitates. Microhardness in HAZ of FSPed+aged sample restored from ~255 in FSPed condition to ~320 HV0.2 in FSPed+aged condition. Microhardness increase in the HAZ arose from re-precipitation of Cr-rich and Al-rich precipitates. The additional precipitation of Al-rich precipitates led to slight improvement in hardness in the HAZ as compared with the as-cast condition (300 HV0.2). In addition, base hardness was also enhanced from ~300 to ~320 HV0.2 after aging due to the precipitation of Al-rich precipitates. As shown in Figure 7, hardness increases are marked by strengthening mechanisms of A, B, and C; each increase was determined by either a single mechanism or a combination of mechanisms.
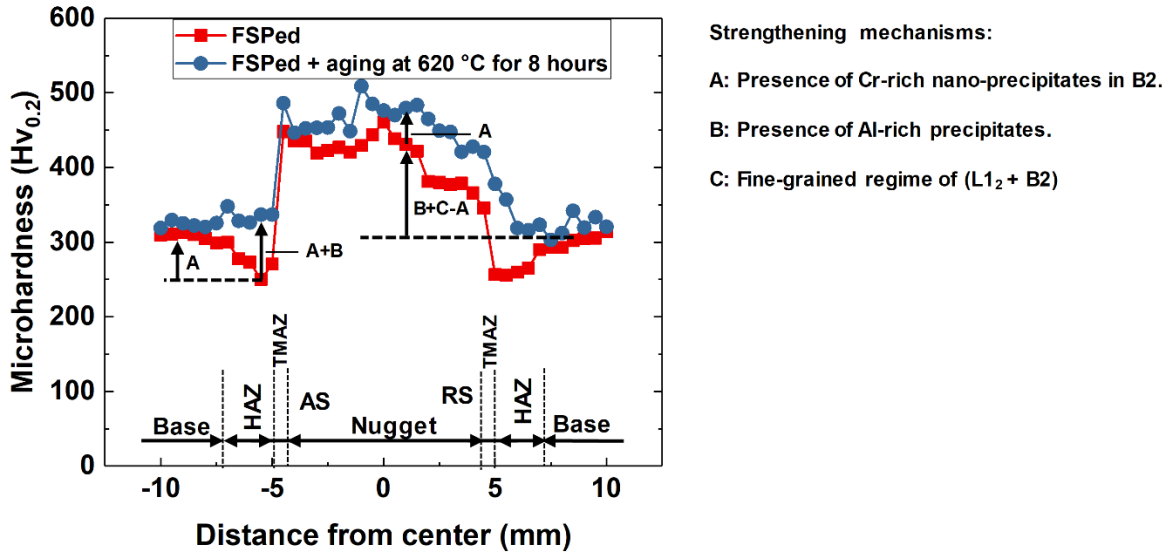
Figure 7. Microhardness profile on the transverse cross section of FSPed and FSPed+aged EHEA specimens.

4. Conclusions

Microstructural evolution and mechanical property characterization of friction stir processed AlCoCrFeNi$_{2.1}$ EHEA led to the following conclusions:

(1) FSP modified the coarse lamellar eutectic structure in the as-cast condition to dynamically recrystallized, ultrafine-grained FCC/L1$_2$ and B2/BCC phases. K-S OR between FCC and B2 phases in as-cast condition was also was reduced after FSP.

(2) Simultaneous enhancement of strength and ductility of EHEA was achieved via FSP. Strength increased due to the formation of ultrafine-grained FCC/L1$_2$ and B2/BCC phases, and ductility increased because of B2 phase refinement.

(3) During FSP, Cr-rich precipitates dissolved in B2 phase in both processed and HAZ regions; while Al-rich precipitates formed in the processed region in FCC/L12 matrix.

(4) Aging heat treatment of 620˚C/8 h led to re-precipitation of Cr-rich precipitates along with the precipitation of Al-rich precipitates in B2 phase.

Acknowledgments

References

[1] J. Yeh, S. Chen, S. Lin, J. Gan, T. Chin, T. Shun, C. Tsau, S. Chang

Nanostructured high‑entropy alloys with multiple principal elements: novel alloy design concepts and outcomes

Adv Eng Mater., 6 (2004), pp. 299-303

[2] J. Yeh, S. Lin, T. Chin, J. Gan, S. Chen, T. Shun, C. Tsau, S. Chou

Formation of simple crystal structures in Cu-Co-Ni-Cr-Al-Fe-Ti-V alloys with multiprincipal metallic elements

Metall Mater Trans A., 35 (2004), pp. 2533-2536

[3] D. Miracle, O. Senkov

A critical review of high entropy alloys and related concepts

Acta Mater., 122 (2017), pp. 448-511

[4] Y. Lu, Y. Dong, S. Guo, L. Jiang, H. Kang, T. Wang, B. Wen, Z. Wang, J. Jie, Z. Cao

A promising new class of high-temperature alloys: eutectic high-entropy alloys

Sci. Rep., 4 (2014), p. 6200

[5] X. Gao, Y. Lu, B. Zhang, N. Liang, G. Wu, G. Sha, J. Liu, Y. Zhao

Microstructural origins of high strength and high ductility in an AlCoCrFeNi$_{2.1}$ eutectic high-entropy alloy

Acta Mater., 141 (2017), pp. 59-66

[6] I. Wani, T. Bhattacharjee, S. Sheikh, Y. Lu, S. Chatterjee, P.P. Bhattacharjee, S. Guo, N. Tsuji

Ultrafine-grained AlCoCrFeNi$_{2.1}$ eutectic high-entropy alloy

Mater Res Lett., 4 (2016), pp. 174-179

[7] I. Wani, T. Bhattacharjee, S. Sheikh, P. Bhattacharjee, S. Guo, N. Tsuji

Tailoring nanostructures and mechanical properties of AlCoCrFeNi$_{2.1}$ eutectic high entropy alloy using thermo-mechanical processing

Mater Sci Eng A., 675 (2016), pp. 99-109

[8] S.R. Sharma, Z. Ma, R.S. Mishra

Effect of friction stir processing on fatigue behavior of A356 alloy

Scr. Mater., 51 (2004), pp. 237-241

[9] A. Feng, Z. Ma

Enhanced mechanical properties of Mg–Al–Zn cast alloy via friction stir processing

Scr. Mater., 56 (2007), pp. 397-400

[10] K.H. Song, K. Nakata

Mechanical properties of friction-stir-welded Inconel 625 alloy

Mater Trans., 50 (2009), pp. 2498-2501

[11] V. Tungala, A. Arora, B. Gwalani, R.S. Mishra, R.E. Brennan, K.C. Cho

Microstructure and mechanical properties of friction stir processed cast Eglin steel (ES-1)

Mater Sci Eng A., 709 (2018), pp. 105-114

[12] M. Komarasamy, R. S. Mishra, S. Mukherjee, M. L. Young

Friction stir-processed thermally stable immiscible nanostructured alloys

JOM, 67 (2015), pp. 2820-2827

[13] M. Komarasamy, N. Kumar, Z. Tang, R. S. Mishra, P. Liaw

Effect of microstructure on the deformation mechanism of friction stir-processed Al$_{0.1}$CoCrFeNi high entropy alloy

Mater Res Lett., 3 (2015), pp. 30-34

[14] S. Asgari, E. El-Danaf, S. R. Kalidindi, R. D. Doherty

Strain hardening regimes and microstructural evolution during large strain compression of low stacking fault energy fcc alloys that form deformation twins.

Metall Mater Trans A, 28 (1997), pp.1781-1795.